Damage and fracture of PVDF at 20°C

Mélanie Challier [(1)], Jacques Besson [(1)], Lucien Laiarinandrasana [(1)], Roland Piques [(1)],Gilles Hochstetter [(2)],Stéphanie Pignoc [(3)]

(1) : Centre P.M.Fourt, Ecole des Mines de Paris, BP 87, 91003 Evry, France
melanie.challier@ensmp.fr
(2) : Atofina, BP 19, 21470 Serquigny (France)
(3) : Technip-Flexifrance, BP 7, 76580 Le Trait (France)

Abstract

Flexible oil pipelines are multilayered structures used for the transport of crude oil or natural gas from the seabed to the surface in offshore oil fields. Because of severe service conditions, composite structure made of metallic and polymeric layers must be used. PVDF is a good candidate as it accommodates tensile and flexural deformations and guarantees watertightness. The present paper focuses on the mechanical properties of PVDF at 20°C. Several specimens with different geometries were tested: notched specimen and cracked specimen under tension. Fracture surfaces were examined to determine fracture mechanisms. Based on mechanical testing and microscopic observations, a modified Gurson-Tvergaard-Needleman model for semi-crystalline polymers is proposed. The model allows to represent the non-linear behavior and the cracking of polymer structures.

1. Introduction

Polyvinylidene fluoride (PVDF) is a semi-crystalline polymer that has been widely studied for its piezoelectric properties, Prest and Luca [1], Holstein et al [2], due to its polar β phase. Nevertheless, the apolar phase α is also studied for structural applications, because it exhibits good mechanical properties and chemical resistance, Castagnet et al [3]. Mechanical properties of PVDF have been already studied by many authors, Castagnet et al [4], Hartman and Lee [5]. The macroscopic tensile and creep behavior was studied over several strain rate decades, and over a large range of temperatures. During viscoplastic deformation, the material whitens after the onset of necking due to nucleation and growth of voids as evidenced by Castagnet [3] using small and large angle X-ray diffraction. In this study, an α-PVDF grade used for offshore application is analysed at 20°C with respect to viscoplastic and damage behavior. Notched and cracked specimens were used in order to investigate damage development over a wide range of loading conditions. A numerical simulation of these tests is performed using the Gurson model [6] which was adapted to the present material.

2. Materials

The material of the study was provided by AtoFina. It is used in a multilayered offshore risers. The material was extruded without plasticizer, and therefore differs considerably from the standard industrial grade. The lack of plasticizer leads to a difficult extrusion, which create a significant porosity. The initial defect population was evaluated by microscopic examination of a PVDF sample broken in liquid nitrogen. The porosity is

equal to 10%. It consists of a 1 μm diameter voids which are always observed in bulk PVDF and that are created during crystallisation and extrusion [4]. A second, much smaller (0.1 μm) population is also observed in the investigated material. It is attributed to the lack of plasticizer and to the difficult extrusion conditions. Due to porosity ratio, this grade is not representative of industrial PVDF behavior. Unplasticized grade could exhibit brittle failure at 20°C , that is not observed with industrial PVDF.

3. Mechanical testing

3.1. Tensile tests on circumferentially notched round bars (CNRB)

Engineering thermoplastics have been found to be significantly notch-sensitive, in that they exhibit a brittle mode of failure in notched specimens, which generate a state of sufficiently large hydrostatics tension ahead of the notch, Gearing and Anand [7]. This stress state also promotes voids growth. In the present work, CRNB tensile tests have been performed using three notch radii : CNRB 4 : R = 4 mm, CNRB 1.6 : R = 1.6 mm, CNRB 08 : R = 0.8 mm. All specimens have a 65-mm length, the diameter in the minimal cross section is 4 mm, and the maximum diameter is 7.2 mm. A strain gage is attached in the vicinity of the notch tip in order to record the decrease of the minimum diameter. The crosshead displacement is also measured (figure 1a). Tests have been carried out by controlling either the crosshead displacement (0.15 mm/s), or the diameter reduction ($2.5.10^{-3}$ mm/s).

Decreasing the notch radius leads to an increase of the maximum load as the stress triaxiality ratio (τ) is increased, Bridgman [8]. Typical results are shown figure 1a for the three notch radii, where the load is plotted versus radial displacement. As expected, fracture occurs sooner with small radii. Results obtained on CNRB 4 and CNRB 1.6 indicate an increase of maximum load. But no similar effect is obtained between CNRB 1.6 and CNRB 08. The maximum load reaches a limit value for radii smaller than 1.6 mm.

In order to check this effect, similar tests were carried out on same geometry under similar conditions with a 0.15 radius (CNRB 0.15). In this case, another radial extensometer is used to fit into the sharp notch. Same maximum load value was obtained. Brittle fracture is observed whereas the other specimens failure mode was ductile. Similar results have been reported in bending on other engineering thermoplastics [7], Ishikawa et al, [9], Narisawa and Yee, [10]. It is shown that fracture becomes brittle when the notch radius is decreased as a constrained plastic zone is formed at the notch root where hydrostatic stresses are high leading to brittle fracture. In conclusion, all results clearly indicate that brittleness is favoured by high triaxiality ratios.

3.2. Double cracked specimen have been tested in tension (DENT).

These tests are carried out to induce more severe loading conditions compared to CNRB specimens. A constrained plastic zone is confined at the crack tip. Specimens are machined from PVDF 12 mm thick extruded sheets (ASTM D638 M1). The length is 100 mm, the width (W) is 6 mm. Various crack length (a) width ratios are used ranging from 0.1 to 0.5. The cracks are made with a cutter blade. Special attention is paid to guarantee alignment of both cracks. Initial crack lengths are measured from the fracture surfaces using an optical microscope. DENT tests are carried out at constant crosshead speed (0.15 mm/s), and a gage extensometer (gage length: 7 mm) is used to follow the crack opening displacement (COD). Figure 1b displays the load versus COD, for a/W ratios between 0.07 and 0.46.

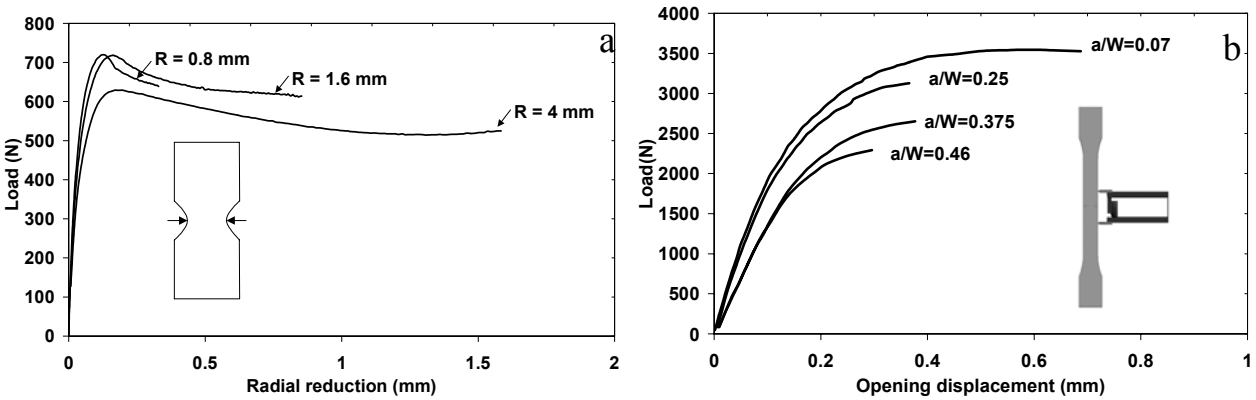

Figure 1 : a. Load-diametrical decrease curves for notched specimens at 20°C at radial decrease $2.5.10^{-3}$ mm/s, b. Load-COD results on DENT, at 20°C and 0.15 mm/s for different a/W ratios.

4. Microscopic Observations

Fracture surfaces of notched specimens have been observed by Scanning Electron Microscopy (SEM). Interrupted tensile tests have been carried out to highlight damage development and localisation. Tensile tests were stopped just prior fracture. Then, the specimens were microtomed along the tensile direction. Optical observations of 2-µm thick lamella and SEM observations of longitudinal cross sections indicated that for the two smaller radii, a localised damage band, containing many cavities, is observed in the minimal cross section (figure 2a). Crazing is not observed and voids are larger at the specimen centre, where stress triaxiality ratio is high. The damage band width decreases for smaller radii.

Fracture surfaces observed in SEM indicates an initiation site located at the centre of the minimum cross section. The macroscopic crack is initiated on a cavity or on a particle (figure 2b). EDX analysis revealed that it is composed of potassium salt or calcium salt. Radial propagation is characterised by many large cavities. Diameter of voids diminishes with propagation, and striations could also be observed at the end of ductile propagation close to specimen edges (figure 2c).

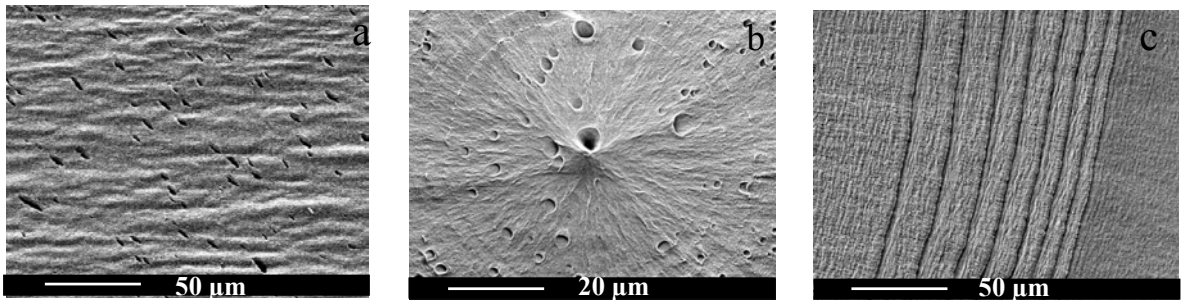

Figure 2 : a. SEM observation of interrupted CNRB 0.8 mm test, b. Initiation site of propagation on CNRB, c . Striations observed during propagation

Optical observations carried out during the DENT test show that the white zone is located at the crack tip indicating that the deformation and damage remain confined. Blunting up to 60 µm prior to crack initiation was observed on test performed in the SEM chamber. Crack initiation is always ductile and quickly followed by unstable brittle fracture (figure 3).

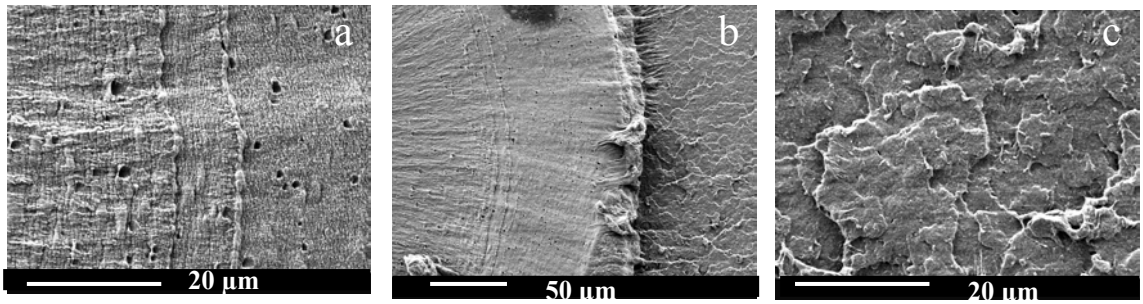

Figure 3 : SEM observations a. Ductile propagation, b. Ductile-brittle transition area, c. Brittle surface

Crack propagation is always larger at the centre of the specimen (tunnelling effect) as plane strain conditions (high stress triaxiality) prevail at this location whereas, plane stress conditions (low stress triaxiality) are met at the free surfaces. The percentage of brittle zone on the fracture surface was evaluated for different a/W ratios. It varies from 70% for a/W = 0.07 to 80% for a/W = 0.46. This is related to the confinement of the crack tip plastic zone which is more pronounced for the long cracks. Striations are also observed close to the ductile-brittle transition zone.

From the study of CNRB and DENT specimens, it is concluded that macroscopic crack initiation is always ductile followed by a stable ductile crack advance. As the crack grows, it becomes unstable so that quasi-static loading conditions do not prevail any longer. Under dynamic conditions, unloading of the crack tip can occur leading to crack arrests which create striations marks as observed under fatigue loading, Hertzberg et al [11]. The observed distance between the striations (10-20 µm) is consistent with observations on fatigued polymers [11]. As the crack speed further increases, stresses are increased, due to the strain rate dependence of the material, so that brittle fracture is triggered.

Microscopic damage process consists of growth of pre-existing voids induced by the deformation of the semi-crystalline matrix. This deformation involves in general the elongation of amorphous tie chains followed by slip and tilting of crystalline lamellar chains, and orientation of crystal blocks, Schultz [12]. Once the spherulites are destroyed and transformed into fibrillar morphology, deformation occurs by destruction of lamellar morphology. This last deformation process induces a strong hardening. Indeed, void growth is enhanced for high stress triaxiality ratios.

5. Damage quantification on notched specimens

As the initial material porosity is high, significant volume variations can be expected during testing. Video acquisition followed by image processing was used for that purpose. This technique has already been used for tensile tests on smooth specimens, Castagnet et al [13], Quatravaux et al [14]. In this study, it was also applied to notched specimens. As shown on figure 4, the outer surface located on both sides of the minimum cross section is painted in black to track its evolution using the video acquisition system. The height of the painted zone is chosen to match the extension of the whitened (i.e. damaged) region. The volume change is then computed for each load step assuming that initially straight cross sections remains straight. This leads to a slight error on the actual volume change. Tests were conducted on CNRB 4 and CNRB 08 samples at a crosshead speed of 0.05 mm/s. Results are shown on figure 4a for a CNRB 4 where the load and the relative volume change $\Delta V/V_0$ are plotted against time. Volume starts to strongly increase slightly before the load maximum, which corresponds to the onset of whitening. For high levels of

deformation, the rate of volume change decreases; at this stage void growth is probably limited by fibrils stretching. Similar conclusion are drawn for tests performed on CNRB 08 specimens. As these measurements involve both effects related to the material behavior and structural effects, they can not be directly interpreted. However, they can be used to adjust the parameters of the constitutive models used to represent deformation and damage behavior (see below).

6. Modelling

The model is based on Gurson's yield function [6], extended by Needleman and Tvergaard [15], [16], Besson et al, [17] to incorporate isotropic hardening, strain rates effect and coalescence. An effective stress, σ* depending on damage is defined by:

$$\Phi\left(\sigma,\sigma^*,f\right)=\frac{\sigma_{eq}^2}{\sigma^{*2}}+2q_1.f.\cosh\left(\frac{q_2\sigma_{kk}}{2\sigma^*}\right)-1-q_1^2f^2 \overset{def.\sigma^*}{=} 0 \tag{1}$$

σ_{eq} is the von Mises stress, and σ_{kk} the trace of the stress tensor. f is the porosity, q_1 and q_2 are model parameters that were introduced to improve the model predictions for periodic arrays of cylindrical and spherical voids. The yield surface is now expressed as $\Phi=\sigma^*-R$ where R is the flow stress of the matrix material. Note that hardening was supposed to be isotropic as the study is only concerned with monotonic loadings. The viscoplastic strain rates tensor, $\underline{\dot{\varepsilon}}$, is given by the normality rule as :

$$\underline{\dot{\varepsilon}}=(1-f)\dot{p}\frac{\partial\Phi}{\partial\underline{\sigma}} \tag{2}$$

so that $(1-f)\dot{p}\sigma^*=\underline{\sigma}:\underline{\dot{\varepsilon}}_p$. $\dot{p}$ is given using the matrix viscoplastic law which will be expressed as a Norton law : $\dot{p}=\left(\frac{\Phi}{K}\right)^n$. The evolution of porosity is expressed using mass conservation $\dot{f}=(1-f)trace\left(\underline{\dot{\varepsilon}}\right)$.

Several parameters need to be identified. The first set is related to the polymer matrix behavior : R,K,n. A second set is used to describe damage evolution : q_1,q_2. As the initial porosity is high, all these parameters need to be adjusted simultaneously. This identification is performed using tensile tests on smooth specimens (not reported here) and tests on CNRB specimens using both the force-displacement curves (§3) and volume variation (§5). The model is validated by simulating the mechanical response of DENT specimens.

Poisson's ratio, ν, was fixed at 0.38, and the young modulus, E, was identified together with the others parameters. The material flow stress is expressed as :

$$R=Q(1-\exp(-bp))+A(\exp(Bp)-1) \tag{3}$$

As $R(p=0)=0$, the material immediately yields. The first term $(Q(1-\exp(-bp)))$ describes the initial hardening stage, i.e. the deformation of the amorphous phase. The second term $(A(\exp(Bp)-1))$ allows to simulate the large stretching of the fibrils which leads to a rapidly increasing stress.

To simulate the post yield softening (fig 4a, 5a), it is necessary to use large values for q_2. As the material deforms, elongated cavities are formed between the fibrils so that their growth rate is decreased [4]. This corresponds to the evolution of the volume change for large deformation respected in §5. Consequently, q_2 was expressed as a function of the maximum principal plastic strain p_1. Note that using large value for q_1, did allow to obtain a good fit of both the load-displacement curves (fig 5a) and the volume variation (fig 4a). Final fracture is assumed to occur when the porosity reaches a critical value f_c.

Optimized parameters are gathered in table 1. Comparisons of experimental and adjusted curves are shown on figures 4,5. Figure 4b compares the experimental and computed deformed shapes of a CNRB 4 sample just before fracture. A good agreement is obtained. In particular, denotching is followed by renotching. From the FE results it can be observed that the originally straight mesh remains straight so that the computed volume variation (§5) corresponds to the actual one. The load plateau observed after the post-yield softening is the result of two opposite effects: (i) void growth (i.e. strong softening), (ii) a chain elongation (i.e. strong hardening). Note that fitting the hardening and damage parameters without considering the volume change data leads too much lower value for q_2, and a less pronounced large strain-hardening. However, the actual volume change is in that case strongly underestimated.

Matrix behavior parameters	Elasticity		Strain rate effect				Flow stress	
	E = 2GPa	ν = 0.38	n = 4.5	K= 15	Q = 52	b=85	A=11	B=1.6
Damage parameters	Void growth					Critical void at fracture		
	$f = 0.1$	$q_1 = 0.8$	$q_2 = \begin{cases} 1.55 \; if \; p_1 < 0.2 \\ 1 + \exp(-3p) \; if \; p_1 \geq 0.2 \end{cases}$			$f_c = 0.6$		

Table 1 : Optimized matrix behavior and damage parameters

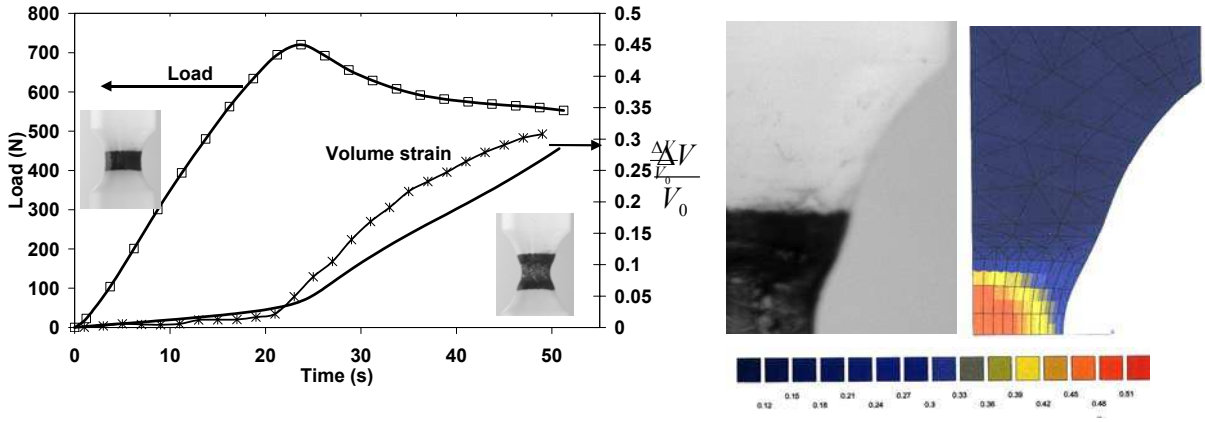

Figure 4 : a. Tensile test performed at 20°C, 0.05 mm/s, on notched specimen with volume change $\Delta V/V_0$ measurement, b. Experimental specimen (a) and (b) porosity ratio in FE, before fracture

DENT specimens are simulated to validate the model. To represent tunnelling it is necessary to use a 3D mesh. Due to the symmetries, only one eighth of DENT is meshed. Calculations were performed using quadratic 20-nodes bricks with reduced integration (i.e. eight Gauss points). Due to the softening characters of the constitutive equation, FE results strongly depend on the mesh size [7]. It is therefore necessary to choose a mesh size to discretise zones where the crack propagates. In this study, the element height in the direction perpendicular to the crack propagation plane is equal to 50 µm. This length was chosen as it approximately corresponds to the width of the highly damaged localisation band observed on figure 2a. Simulated load/crack-mouth opening curves are compared to experimental data on figure 5b showing a good agreement, for the maximum and minimum values of the a/W ratios. Simulation indicates that the macroscopic crack is initiated at the load maximum. As experimentally observed (figure 6a, 6b), stable crack growth is simulated for a crack advance between 0.2(W-a) and 0.3(W-a) (figure 6c). At this point, the load rapidly decreases which corresponds to the experimentally observed onset of instability. The model can no longer be applied as it does not account for: (i) dynamic effects, (ii) adiabatic heating, (iii) ductile to brittle failure transition.

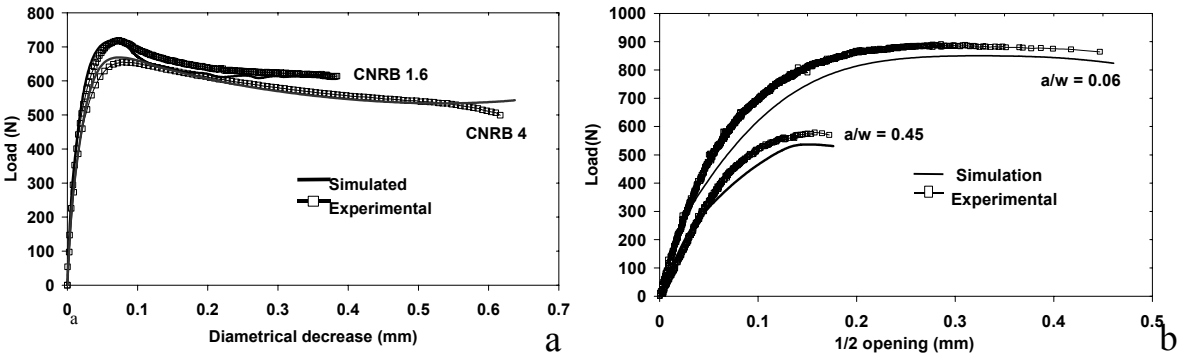

Figure 5 : a. Simulated-experimental load versus diametrical decrease, for CNRB 4 and CNRB 16, at 20°C, b. Simulated-Experimental Load-1/2 opening in DENT

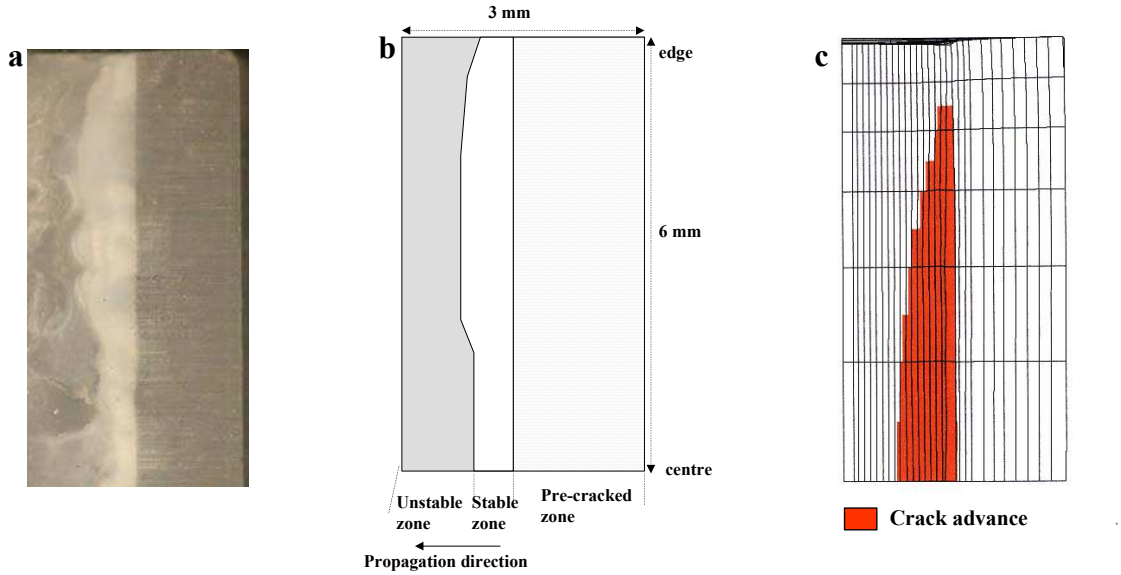

Figure 6. Experimental (a,b) and simulated (c) crack propagation for a 0.5 a/W ratio, during DENT test

Conclusion

Viscoplastic and damage behavior of a unplasticized PVDF has been studied using different test geometries. Mechanical tests corroborated by fracture surface examinations and volume change measures indicate that damage is essentially caused by void growth. Softening by void growth and strain-hardening by chains elongation occur simultaneously. A constitutive model accounting for both effects is employed to represent the mechanical behavior of the material. It is adjusted on tests carried out on smooth and notched tensile bars. It is validated on DENT specimens in which stable crack growth occurs.

References

1. Prest, W. M, Luca, D. J., J. of applied physics, Vol 46, N°10, October 1975
2. Holstein,P., Scheler, U., Harris, R., Polymer Vol 39, N° 20, pp 4937-4941, 1998
3. Castagnet, S., Girault, S., Gacougnolle, J.L., Dang, P., Polymer 41, (2000), 7523-7530
4. Castagnet, S., Thesis, *comportement mécanique du PVDF : competition entre cavitation et ecoulement visqueux,* Poitiers, 1998
5. Hartman, B. , Lee, G. F., Polym. Eng. Sci. 31 (1991) 231-238
6. Gurson, A.L., J. Of Eng. Mat. and Tech., 1977-99, 2-15
7. Gearing, B.P., Anand, L., Int.J of solids and structures 41 (2004), 827-845
8. Bridgman, P.W, Trans. Amer. Soc. Met.,32, (1944), p 553
9. Ishikawa, M., Narisawa, I., Ogawa., H. Journal of polymer Science 15, 1977, 1791-1804
10.Narisawa, I., Yee, A.F., in Materials Science and Technology. A comprehensive Treatment 12, 1993, 699-765
11. Hertzberg, R. W., Manson, J. A., Skibo, M. D., : Polymer Engineering and Science. 15, 252 (1975)
12. Schultz, J., Mechanical Behavior of semi-cristalline polymeric materials, Polymer materials Science, Prentice-Hall, Englewood cliffs, 1974, Chapter 11, 4661
13. Castagnet, S., Gacougnolle, J.L., Dang, P., Mat. Sci. And Eng. A276 (2000) 152-159
14. Quatravaux, T., Elkoun, S., G'Sell., C, Cangemi, L., Meimon, Y., J. of Pol. Sci., Part B : Polymer Physics, Vol 40, 2516-2522, (2002)
15. Tvergaard, V., Advances in applied mechanics 27, 1990, 83-151
16. Tvergaard, V., Needleman, A., Acta Metallurgica, 32, 1984, 157-169
17. Besson, J., Steglich, D., Brocks, W., Int. J. o Sol. And Struc. 8259-8284, 2001